GeroScience
https://doi.org/10.1007/s11357-023-00830-5

ORIGINAL ARTICLE

Long-term dasatinib plus quercetin effects on aging outcomes and inflammation in nonhuman primates: implications for senolytic clinical trial design

Alistaire D. Ruggiero · Ravichandra Vemuri · Megan Blawas · Masha Long · Darla DeStephanis · Abigail G. Williams · Haiying Chen · Jamie N. Justice · Shannon L. Macauley · Steven M. Day · Kylie Kavanagh

Received: 9 February 2023 / Accepted: 17 May 2023

Abstract Cellular senescence increases with aging and results in secretion of pro-inflammatory factors that induce local and systemic tissue dysfunction. We conducted the first preclinical trial in a relevant middle-aged nonhuman primate (NHP) model to allow estimation of the main translatable effects of the senolytic combination dasatinib (D) and quercetin (Q), with and without caloric restriction (CR). A multi-systemic survey of age-related changes, including those on immune cells, adipose tissue, the microbiome, and biomarkers of systemic organ and metabolic health are reported. Age-, weight-, sex-, and glycemic control-matched NHPs (D + Q, $n = 9$; vehicle [VEH] $n = 7$) received two consecutive days of D + Q (5 mg/kg + 50 mg/kg) monthly for 6 months, where in month six, a 10% CR was implemented in both D + Q and VEH NHPs to induce equal weight reductions. D + Q reduced senescence marker gene expressions in adipose tissue and circulating PAI-1 and MMP-9. Improvements were observed in immune cell types with significant anti-inflammatory shifts and reductions in microbial translocation biomarkers, despite stable microbiomes. Blood urea nitrogen showed robust improvements with D + Q. CR resulted in significant positive body composition changes in both groups with further improvement in immune cell profiles and decreased GDF15 ($p = 0.05$), and the interaction of D + Q and CR dramatically reduced glycosylated hemoglobin A1c ($p = 0.03$). This work indicates that 6 months of intermittent D + Q exposure is safe and may combat inflammaging via immune benefits and improved intestinal barrier function. We also saw renal benefits, and with CR, improved metabolic health. These data are intended to provide direction for the design of larger controlled intervention trials in older patients.

Keywords Senolytics · Caloric restriction · Inflammation · Adipose tissue · Leaky gut

Alistaire D. Ruggiero and Ravichandra Vemuri have equal contributions.

Supplementary Information The online version contains supplementary material available at https://doi.org/10.1007/s11357-023-00830-5.

A. D. Ruggiero · R. Vemuri · M. Blawas · M. Long · D. DeStephanis · A. G. Williams · K. Kavanagh (✉)
Department of Pathology, Wake Forest University School of Medicine, Winston-Salem, NC, USA
e-mail: kkavanag@wakehealth.edu

H. Chen
Department of Biostatistics and Data Science, Wake Forest University School of Medicine, Winston-Salem, NC, USA

J. N. Justice · S. L. Macauley · S. M. Day
Section of Gerontology and Geriatric Medicine, Department of Internal Medicine, Wake Forest University School of Medicine, Winston-Salem, NC, USA

K. Kavanagh
College of Health and Medicine, University of Tasmania, Hobart, TAS, Australia

Published online: 01 June 2023

Introduction

Aging is defined by progressive loss of physiological integrity, which increases the risk of chronic diseases, including cardiovascular disease, cancer, Alzheimer's disease, and type II diabetes [1]. Key molecular pathways that converge and induce dysfunction with aging and contribute to the development of chronic diseases include genomic instability, loss of proteostasis, mitochondrial dysfunction, disordered nutrient sensing, and cellular senescence [2]. Cellular senescence is a dysfunctional state caused by stressors including DNA damage, inflammation, and metabolic dysfunction [3]. Senescent cells avoid apoptosis by taking advantage of senescent cell anti-apoptotic pathways [4] while simultaneously secreting pro-inflammatory and pro-fibrotic factors as part of their senescence-associated secretory phenotype (SASP). This results in dysfunctional extracellular matrix formation and neighboring cell senescence with propagation of inflammatory processes [5].

Through transcriptomic analyses of senescent versus non-senescent human cells including preadipocytes, dasatinib (D), a tyrosine kinase inhibitor, and quercetin (Q), a naturally occurring flavonoid, were found to induce apoptosis of senescent cells [4]. Specifically, D was identified to preferentially target senescent preadipocytes while Q was found to preferentially target senescent endothelial cells in vitro [4]. A 30% reduction in senescent cells suffices to alleviate dysfunction in preclinical models [6]. Recently, use of pharmacological senescent cell clearing agents have demonstrated improved healthspan in rodent models [7–9] and some positive effects in short-term clinical pilot assessments [10, 11]. When used in combination, intermittent administration of D + Q successfully reduced human adipose tissue senescent cell burden [11], macrophage accumulation [11], and secretion of SASP factors [12]. It likewise improved physical function in people [12], and improved healthspan [4], intestinal barrier function, and glucose tolerance in mice [13]. It is thought that the use of senolytics could alleviate age-related adipose tissue and system metabolic dysfunction, though a placebo-controlled trial in people has not yet been conducted. However, senolytics in combination with lifestyle modification — the clinical standard of care for prevention of health events in middle-aged and older adults with metabolic syndrome and gold standard for health and lifespan extension in animal models — has not been examined.

To date, caloric restriction is the gold standard for improving healthspan and metabolic dysfunction. It is well-established that caloric restriction (CR) slows the onset of age-associated diseases and extends lifespan and healthspan in animal models, including primates. A 20–30% CR has been shown to improve immune function [14, 15], motor coordination [16], muscle mitochondrial function [17], reduce sarcopenia [18], resting metabolic rate [19], and mortality [19]. In addition to these health benefits, CR reduces tissue senescent cell burden [20]. Although potentially efficacious, many adults are either not adherent to lifestyle changes or not responsive to CR alone, prompting a need to evaluate combination CR and pharmacologic therapies on metabolic and aging outcomes. Moreover, less discussed are the negative or neutral effects of CR which can include shortened lifespans, reduced thyroid hormone levels, and loss of lean and bone mass and even grey matter in the brain, bolstering the need for alternative interventions for health with aging.

It is unknown how D + Q senolytic therapy and CR compare or synergize for the treatment of age-related metabolic dysfunction. In this study, we evaluated the safety and efficacy of monthly intermittent D + Q administration alone and when combined with low-percentage caloric restriction (10%) for 6 months, a duration relevant to human clinical trial design. We assessed changes in metabolic syndrome risk factors, body composition, circulating SASP/inflammation and Alzheimer's disease biomarkers, serum biochemistry and immune cells, microbiomes, and local adipose tissue macrophage accumulation. We hypothesized that systemic reductions in senescent cell burden would improve cardiometabolic outcomes and reduce inflammation and related immune cell phenotypes. We find that D + Q does induce improvements in healthspan markers relating to the immune, gastrointestinal, and renal systems and, combined with CR, induces some unique benefits and synergisms. This study provides the fundamentals to relating in vivo exposure to the effects of senolytics and/or CR and provides data relevant to the design of a larger randomized controlled trial.

Methods

Nonhuman primate cohort

A total of 16 male and female cynomolgus macaques (*Macaca fascicularis*) were selected for this work. Animals in the control and treatment groups were matched by age, sex, body weight, glycemic control, and metabolic syndrome risk factors (Supplementary Table 1). Animals were middle-aged (roughly 45 in human equivalent years) and ranged from lean to obese, where obesity was defined by a waist circumference of > 40 cm and a percent body fatness of > 30% measured from computed tomography (CT) image analyses [21, 22]. Animals were normoglycemic to type II diabetic. Three animals diagnosed with type II diabetes were included in each group. Consistent with the American Diabetes Association definition, animals were diagnosed as diabetic after two or more fasting blood glucose measures of ≥ 126 mg/dL and glycosylated hemoglobin A1c (A1c) value > 6.5% [23]. Insulin therapy was provided twice daily to those animals, with doses determined using postprandial glucose levels as previously described with A1c values ranging 6.3–8.8% at study initiation [23]. Insulin therapy had been consistent for ≥ 3 months prior to study start and were considered moderately well-controlled being weigh stable and A1c < 9% All animals were socially housed indoors with equal access to exercise and consumed a laboratory chow diet that was low in saturated fats and simple carbohydrates, and high in protein and fiber (Laboratory Diets 5038; LabDiet, St. Louis, MO) throughout the study, with dietary caloric restriction of this diet instituted in the sixth month of study (Fig. 1).

All described procedures were performed according to the National Institutes of Health Guide for Care and Use of Laboratory Animals. All study procedures were approved by and performed in accordance with the Wake Forest University Institutional Animal Care and Use Committee. An overall schema depicting the study design and collections is shown in Fig. 1.

Food consumption assessment and caloric restriction

At baseline and 5 months, all study animals had their food consumption measured. For three consecutive days animals were fed excess calories (100 kcal/kg) once daily and food amounts were weighed at the beginning and end of each 24-h period. We determined that there were no differences in consumption (Supplementary Table 2). Immediately after administration of dose six (at 5 months), animals underwent a 10% caloric restriction for 6 weeks. The restriction food amount was determined using the average caloric intake each individual was consuming at month five, with 90% of this being supplied daily for the final 6 weeks of the study. During the caloric restriction, animals were provided enrichment, which included celery and cucumbers considered to have insignificant caloric contributions. After caloric restriction, animals had their bodyweights measured weekly to confirm weight loss and CT imaging was repeated after 6 weeks. In total, all study animals experienced

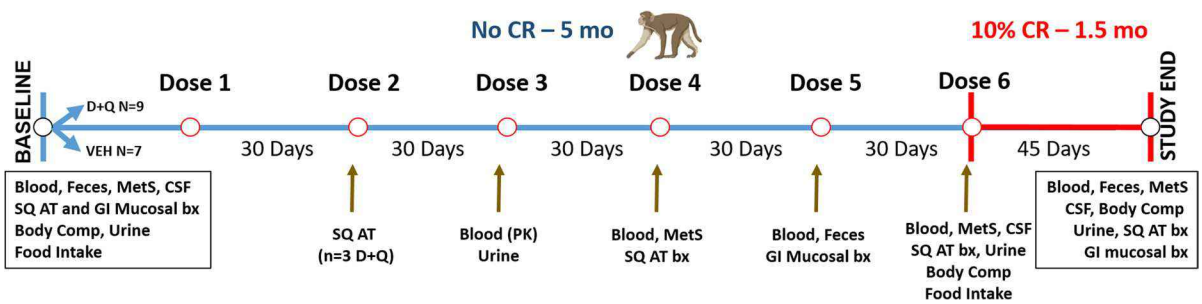

Fig. 1 Overview of study timeline and outcome measures. Demographic details are shown in Supplemental Table 1. Seven vehicle (VEH) treated control and nine Dasatinib (D) and Quercetin (Q) treated middle-aged cynomolgus macaques were included in study. Study outcomes and timing are shown relative to ad libitum (No CR) and caloric restriction (CR) phases. Samples were collected and included those relating to metabolic syndrome (MetS) criteria, cerebrospinal fluid (CSF), subcutaneous (SQ) adipose, and gastrointestinal (GI) colon mucosal biopsies (bx), feces and blood. Computed tomography imaging was performed to determine body composition (Body Comp) to confirm the effects of the feeding phases

an average of 5% body weight loss, which did not differ between D + Q or vehicle-exposed control groups (Supplementary Fig. 1).

Dasatinib and quercetin dose administration and pharmacokinetic assessment

All study animals underwent oral gavage of either dasatinib ([D]; Bristol Meyers Squibb, New York, NY) or quercetin (Q; Micro Ingredients, Diamond Bar, CA) or vehicle. Animals were briefly sedated with ketamine (3 mg/kg) and dexmedetomidine (0.035 mg/kg), and NHPs in the treatment group were dosed on two consecutive days once per month with D (5 mg/kg) and Q (50 mg/kg) mixed in Ensure®, whereas control group animals received comparable volumes of Ensure® as vehicle.

To measure circulating concentrations of D and Q parent compounds and metabolites, blood samples were drawn exactly 2 h post-oral administration to estimate maximal concentrations at the 3rd dose (mid-study). Blood samples were immediately processed for plasma, and plasma samples were stored at − 80 °C until analyses. Concentrations of D and its metabolites were calculated by mass spectrometry of unknowns and standards. Concentrations of Q and its metabolites were processed by the Biological Psychiatric Analytical Laboratory at the University of Texas Health, San Antonio.

Body composition analyses

CT scans were performed at baseline, and after 5 and 6 months of treatment, using a Siemens SOMATOM Definition Flash CT scanner (Siemens, Munich, Germany). These scans were reconstructed as DICOM images using Aquarius Net Thin Client (TeraRecon, Durham, NC), and then analyzed using Materialise's Interactive Medical Image Control System (Mimics) (Materialise, Leuven, Belgium). Fat and lean tissues were identified using pre-determined voxels [24], from which whole body tissue volumes were determined, adjusted for density, and expressed as a percentage of the animal's body weight, as well as a fat-to-lean tissue ratio. The abdominal region was defined through segmentation from the thoracolumbar junction to the sacroiliac junction to assess the intra-abdominal and subcutaneous fat tissue volumes [21]. These volumes were adjusted for density and expressed as tissue mass, as well as an intra-abdominal-to-subcutaneous ratio [21]. At least three liver attenuation measures by circular ellipse were averaged. Psoas lean tissue area and attenuation were collected by tracing the circumference of the lean tissue at the L4 vertebra [21]. Mid-thigh lean tissue area and attenuation were measured by tracing the circumference of the lean tissue at the midpoint between the greater trochanter and patella.

Metabolic syndrome risk criteria and blood measures

All samples described below were collected in the morning, after 12 h fasting and, in the diabetic individuals, after a 16-h withdrawal from exogenous regular short-acting insulin administered at the prior afternoon's meal. All samples and measures were collected at the end of the D + Q dose period prior to administration of the next dose. Animals had their waist circumferences measured using a flexible tape measure at the level of the umbilicus [25]. Blood pressure was measured indirectly using a sphygmomanometer with digital high-density oscillometry readouts where the average of three measures was calculated [26]. Blood samples were collected using percutaneous femoral venipuncture and urine samples were collected via cystocentesis at baseline, 3 months, 5 months, and 6 months. Blood was collected into ethylenediaminetetraacetic acid (EDTA) tubes and placed on ice until processed for plasma. Plasma aliquots were stored at − 80 °C until analyzed. Triglyceride (TG), high density lipoprotein cholesterol (HDLC), and total cholesterol concentrations were measured enzymatically [25]. Fasting glucose was measured using the glucose oxidase method as previously described [25]. Blood samples were submitted to IDEXX Laboratories for complete blood counts and serum biochemical analyses. Circulating concentrations of monocyte chemoattractant protein (MCP)-1 (R&D Systems, Minneapolis, MN, cat. no. DCP00), interleukin (IL)-6 (R&D Systems, Minneapolis, MN, cat. no. DLB50), growth/differentiation factor (GDF)-15 (R&D Systems, Minneapolis, MN, cat. No. DGD150), C-reactive protein (CRP) (Alpco Diagnostics, Salem, NH, cat. no. 30-9710S), N-terminal (NT)-pro hormone BNP (NT-ProBNP) (My BioSource, San Diego, CA, cat. no. MBS009046), plasminogen activator inhibitor (PAI)-1 (R&D Systems, Minneapolis, MN, cat. no. DSE100),

lipopolysaccharide binding protein (LBP)-1 (LSBio Inc. Seattle, WA, cat. no. LS-F17912), fatty acid binding protein (FABP)-1 (LSBio Inc. Seattle, WA, cat. no. LS-F43728), and immunoglobulin (Ig) A (Mabtech Cincinnati, OH, cat. no. 3860 M-1H-6) were measured in collected plasma or serum samples via enzyme-linked immunosorbent assay (ELISA) and measured in duplicate. A customized Luminex panel of 14 biomarkers relating to the SASP was created and run on serum (R&D Systems) on a Luminex 200 (Luminex Corporation, Austin, TX).

Adipose and mucosal tissue biopsies

Animals were sedated with ketamine (10 mg/kg), intubated, and maintained on isoflurane and placed in lateral recumbency. Subcutaneous adipose samples were collected at baseline, 3 months, 5 months, and 6 months. Endoscopically retrieved descending colon mucosal biopsies were collected at baseline and 5 months. Adipose tissue was collected from adjacent to the umbilicus and colon mucosa from the intersection of the transverse and descending colon. Tissues were either flash frozen or fixed in 4% paraformaldehyde (PFA) until downstream analyses.

Histology and immunohistochemistry

PFA-fixed, paraffin-embedded adipose tissues were used to create four-micron histologic sections. Histological sections were stained with hemotoxylin and eosin. Adipocyte sizes were evaluated using a specialized Visiopharm software (Hoersholm, Denmark) macro that calculated average adipocyte size, total tissue area, total nuclei count, individual adipocyte size, and total adipocyte number. Sections were stained with fluorescent CD68 and CD163 to evaluate total macrophage infiltration (AbD Serotec Bio-Rad, Raleigh, NC), and co-stained with pSTAT1 (Cell Signaling Technology, Danvers, MA) CMAF (Abcam, Cambridge, UK), or both pSTAT1-CMAF markers to identify undefined, M1, intermediate, and M2 macrophages as previously described [27]. P21 protein expression was evaluated via immunohistochemical detection (1:100 dilution; Abcam cat. no. ab109520) in adipose tissue sections. A specialized Visiopharm software (Hoersholm, Denmark) macro was used to identify nuclei positively co-stained with the anti-p21 antibody.

Enzymatic assessments

Senescence-associated beta galactosidase staining was performed at baseline, 5 months, and 6 months. The Cell Signaling Technologies Senescence-Associated β-galactosidase (SA-βgal) Staining Kit (cat. no. 9860S; Danvers, MA) was used according to the manufacturer's instructions to stain 50 mg explants of subcutaneous adipose as previously described [22]. The tissues were incubated in a non-CO_2 incubator for 16–18 h. As the SA-βgal staining solution is pH-sensitive, tissue explants stained using a solution pH of greater than 6 were used as negative controls and explants stained in a solution with a pH of less than 6 were used as positive controls. A total of nine tissue pieces per animal were scored. Four blinded reviewers evaluated the explant staining. SA-βgal staining was scored on a 0 to 5 scale, as previously published [22], where a 0 represented no blue stain and a 5 represented a very dark blue stain.

RNA extraction and gene expression

Expression levels of the senescence markers *CDKN2A* and *CDKN1A* (p16 and p21 genes respectively) were measured. Roughly 100 mg of frozen adipose tissue was homogenized in QIAzol (Qiagen, Hilden, Germany, cat. no. 79306) with a Polytron PT 1200 for 20-40 s. RNA was extract from homogenized adipose tissue with the Qiagen RNeasy Mini Kit (Hilden, Germany, cat. no. 74104). One microgram of RNA was reverse transcribed to cDNA using the Qiagen QuantiTect Reverse Transcription Kit (Hilden, Germany, cat. no. 205313). RT-qPCR was performed using 50 ng of cDNA and the Sigma FastStart Universal SYBR Green ROX Master Mix (Sigma-Aldrich, St. Louis, MO, cat. no. 04913914001). NHP-specific *CDNKN1a* (p16 ^{Ink4a}) and *CDKN2a* (p21) primers that were designed in-house were used. The sequences of the primer sets were the following: p16 ^{Ink4a}: 5'-GCT GCG TCA CTT CTA GCT TC-3' (forward) and 5'-CCA ACT GGG ACA CAC TTG CT-3' (reverse), and p21: 5'-ACT CTC AGG GTC GAA AAC GG-3' (forward) and 5'-TGT GGG CTG ATT AGG GCT TC-3' (reverse). Samples were run on the Applied Biosystems (Waltham, MA) 7500 Fast Real-Time PCR System. Gene expression data were analyzed using the $2^{-\Delta\Delta ct}$ method.

Select apoptosis and necrosis markers were measured using TaqMan Multiplex GEx (Thermo Fisher Scientific, Waltham, MA). Primer/probe combinations were generated for *BCL-2* (*JUN-QSY*), *MLKL (VIC-MGB)*, *BAX (ABY-QSY)*, and 18 s. These genes were measured using reverse transcribed cDNA. Samples were run on the Applied Biosystems (Waltham, MA) 7500 Fast Real-Time PCR System. Gene expression data were analyzed as stated above. All gene expression assessments were performed in triplicate.

Flow cytometric analyses

Peripheral blood mononuclear cells (PBMCs) were isolated from whole blood using Ficoll-Paque density gradients. PBMCs were suspended in freezing media (DMEM with 40% BSA and 15% DMSO) and frozen at –80 °C until analyzed. Frozen PBMCs were removed from storage and thawed in a 37 °C water bath until small amounts of ice remained in the tubes. Thawed cells were transferred to a 50-mL conical tube and supplemented with 1 mL of Dulbecco's Modified Eagle's Medium (DMEM) with 10% fetal bovine serum (FBS) and 50units/mL of Benzonase ([cat no. E1014-25KU], Millipore Sigma, Burlington, MA). The volume was brought to 15 mL using DMEM with 10% FBS, and cells were spun for 10 min at 1500 rpm at room temperature. The supernatant was decanted, cells were resuspended in 15 mL DMEM with 10% FBS, and spun again for 10 min at 1500 rpm at room temperature. After, cells were stained using the following antibody cocktail for 30 min at 4 °C protected from light: anti-CD3-APC-Cy7 (clone 10D12), anti-CD20-Brilliant Violet 510 (clone 2H7), anti-CD45-PE-Cy7 (clone D058-1283), anti-CD14-PE (clone M5E2), and anti-CD16-Brilliant Violet 605 (clone 3G8) BD Biosciences, San Jose, CA, USA). All antibody clones were verified using the Nonhuman Primate Reagent Resource (https://www.nhpreagents.org/ReactivityDatabase). Analyses were performed on a LSR Fortessa X-20 and with FCS Express v.7 software (BD Biosciences, Haryana, India). Human TruStain FcX Fc receptor block (cat. no. 422302), True-Stain Monocyte Blocker (cat. no. 426102, BioLegend, San Diego, CA), the Live-or-Dye Viability Kit (cat. no. 32002, Biotum, Freemont, CA), UltraComp eBeads Compensation Beads (cat. no. 01-2222, Invitrogen, Carlsbad, CA), and fluorescence-minus-one and unstained cell controls were used. The gating strategy used goes as follows: single cells were first identified using forward scatter height (FSC-H) versus forward scatter area (FSC-A). Single cells were then gated on FSC-A versus side scatter area (SSC-A) to remove cell debris. Next, live cells were selected gating SSC-A versus BUV395. $CD45^+$ cells were selected from the live cells. $CD20^+$ and $CD3^+$ cells were removed from $CD45^+$ cells. CD14 and CD16 were then used to identify monocyte subtypes from $CD45^+CD20^-CD3^-$ cells. All cytometric analyses were performed in duplicate.

Microbiome determinations

DNA was extracted from fecal samples and colonic mucosal biopsy specimens. DNA was also extracted from control samples of laboratory air and water collected at the same time as biospecimens were collected (Qiagen QIAmp DNA mini kit, cat. no. 51304). DNA was sequenced (Illumina Inc., San Diego, CA cat. no. MS-102-2003) at 2×250 k reads per sample in a single run for paired end sequencing and libraries prepared using the Illumina 16S V3-V4 kit. Samples were pre-processed, quality filtered and aligned using BaseSpace application 16S Metagenomics (1.1.0) on Illumina®, which was trained for the applied primers using the 99% OTU data set of the Green genes taxonomy release as previously described [28]. Subsequently, taxonomy and generated feature tables were analyzed to estimate alpha (α) diversity profiles to measure species richness, and evenness was analyzed using Shannon's and Simpson's indexes. To determine the microbial variation using beta (β) diversity between the groups, we used clustering methods, such as principal coordinate analysis (PCoA), which were generated with weighted and unweighted UniFrac β diversity metrics. The statistical significance of the differences in β diversity between the groups and sample types was tested with the permutational multivariate analysis of variance (PERMANOVA) test, using the unweighted UniFrac distance matrix as an input and corrected for false discovery rates (FDRs). To confirm that no microbial taxa were differentially abundant between groups, linear discriminate analysis (LDA) effect size (LEfSe) analyses were performed.

Alzheimer's disease biomarkers

Cerebrospinal fluid (CSF) samples were collected at baseline, at 5 months of D + Q and after CR by percutaneous puncture of the atlanto-occipital space in the morning after 12-h fast and a 16-h withdrawal from all exogenous insulin [29]. Concentrations of amyloid β $(Aβ)_{40}$ and $Aβ_{42}$ in CSF samples were assayed using sandwich ELISAs as previously described [29–31]. $Aβ_{40}$ and $Aβ_{42}$ were quantified using monoclonal capture antibodies against amino acids 33–40 (HJ2, $Aβ_{40}$) or 37–42 (HJ7.4, $Aβ_{42}$) that were gifted by David Holtzman [29]. $Aβ_{40}$ and $Aβ_{42}$ used a biotinylated monoclonal antibody against the central domain 13–38 (HJ5.1B) for detection. Super Slow TMB (Sigma Aldrich, St. Louis, MO) was used for assay development, and plates were read on a Bio-Tek (Winooski, VT) Synergy 2 plate reader at 650 nm as previously described [29].

Statistical analyses

All endpoints were evaluated for normality and homogeneity of variance assumptions using Shapiro-Wilk and Levene's tests. Endpoints that did not meet assumptions (TG, PAI1, CRP, intermediate monocyte counts, uPAR) underwent logarithmic transformation. A mixed effects model was used to evaluate (1) the effects of group assignments at baseline, 3 months and 5 months, (2) the effects of CR alone at month six, (3) the effects of treatment alone at month six, and (4) the interaction between treatment and CR. Analyses were adjusted for baseline values and the effects of time. For outcomes that were measured only at month 5, analysis of covariance (ANCOVA) models were fit with the main effect of treatment while adjusting for baseline (pre-randomization) measures. For outcomes that were measured longitudinally post-randomization, linear mixed effects models (LMM) were fit to account for the correlation between repeated measures over time. The models included the main effect of treatment, time point, and the treatment by time point interaction while adjusting for baseline (pre-randomization) measures. Treatment effect was estimated at each time point including month 6 that represented the CR phase. Linear contrasts were constructed to (1) estimate the mean outcome levels prior to CR (post-randomization through month 5) and post-CR (at month 6) in treatment and control groups; (2) estimate the overall treatment effect for the entire duration of the trial with and without CR (post-randomization through month 6); (3) test the effect of CR; and (4) test the treatment by CR interaction. Significant p-values were considered $p \leq 0.05$ and trends were considered $p \leq 0.10$. Microbiome diversity statistical analyses were performed using GraphPad Prism 10 (San Diego, CA) and R (4.1.1).

Pre-determined power analyses using previously collected data indicated that we would have 80% power to detect a 0.75 difference in A1c means between groups with $n = 6$ per group. Post-hoc power analyses using our A1c data and our group numbers indicated that we achieved 80% power to detect a 0.96 difference in means between groups.

Results

Changes in senescence biomarkers and in vivo concentrations of D and Q

To confirm that the intermittent dosing was effectively clearing senescent cells, we evaluated multiple markers including changes in cell cycle inhibitor gene and protein expressions, senescence associated beta-galactosidase (SA-βgal) staining of whole adipose tissue, changes in apoptosis-related gene expression, and circulating SASP markers. Subcutaneous adipose tissue p16 ($p = 0.05$; Fig. 2a) and p21 ($p = 0.04$; Fig. 2b) gene expression was significantly decreased at three months in the animals that received D + Q treatment. The reductions were consistent with results showing that p16 and p21 subcutaneous adipose tissue gene expression were 30–90% decreased at 1 month after D + Q in three animals (Supplementary Fig. 2a and b). No significant changes in either SA-βgal staining (Supplementary Fig. 3a) or p21 protein immunohistochemical staining (Supplementary Fig. 3b) were observed prior to the start of caloric restriction. Caloric restriction significantly increased p21 protein expression ($p = 0.04$; Supplementary Fig. 3b), and a trend toward an interaction between D + Q and CR was observed ($p = 0.09$). However, although CR unexpectedly increased p21 expression, PAI1 and MMP-9, SASP markers previously determined to associate with aging in this model [32], was significantly decreased in animals receiving D + Q compared to those receiving vehicle at month

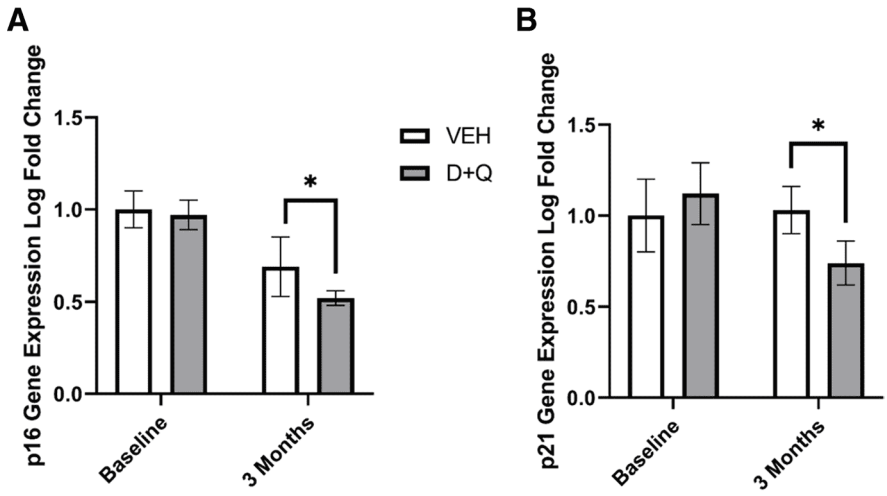

Fig. 2 Senolytic therapy reduces senescent cell burden. Subcutaneous adipose tissue (**A**) p16 and (**B**) p21 gene expression was significantly decreased after 3 months of intermittent dasatinib (D) and quercetin (Q) administration ([$n=9$]; $*=p<0.05$) compared to the tissue of those receiving vehicle (VEH; $n=7$). All values presented are adjusted means ± SEM

six ($p=0.05$; Supplementary Fig. 3c and 3d, Supplementary Table 5). Apoptosis markers were increased in adipose alongside D + Q-mediated decreases in senescent cell markers (Supplementary Fig. 4). The apoptosis-related gene BAX was significantly higher in the subcutaneous adipose tissue of animals treated with D + Q compared to those that received vehicle (VEH) at 5 months ($p<0.05$), and D + Q-treated adipose demonstrated a non-significant increase in BAX expression at 6 months with the addition of CR (Supplementary Fig. 4a). Expression change in BCL-2 was similar to that of BAX ($p<0.1$; Supplementary Fig. 4b). Ratios of BAX/BCL-2 remained higher in the D + Q subcutaneous adipose samples compared to VEH throughout the study, though the ratios did not reach statistical significance (data not shown). No significant changes were observed in MLKL gene expression; however, the expression pattern was consistent with increased cell death in D + Q treated animals undergoing CR (Supplementary Fig. 4c). Differences in the adipose senescent burden of the 3 diabetic individuals are shown in Supplementary Table 5 without statistical inferences as sample sizes are too small. Diabetes did result in an increase in p21-markers and although only 3 animals were exposed to D + Q, three-fold greater reductions in these markers were reported than their non-diabetic counterparts suggesting this population is poised to benefit more from senolytic therapies.

As in vivo concentrations of D and Q and their metabolites have yet to be determined in senolytic studies, we chose to measure the maximal concentrations of these agents and their metabolites in circulation. Neither dasatinib nor dasatinib N-oxide was detected in samples collected from animals receiving vehicle. In the treated group, detectable concentrations of Dasatinib were found in seven of nine animal samples, while detectable levels of Dasatinib N-Oxide were found in four of nine (Supplementary Table 3). On average, 0.12 μM of Dasatinib and 0.019 μM of dasatinib N-oxide were detected in circulation (Supplementary Table 3). Concentrations of Q and Q metabolites were below the limits of detection.

Immune cell and inflammatory shifts with senolytic treatment and caloric restriction

As aging, obesity, and metabolic disease increase circulating and adipose tissue-resident immune cells and pro-inflammatory cytokine signaling, we assessed shifts in white blood cells and adipose tissue macrophage subtypes with senolytic treatment and CR. Overall there was an anti-inflammatory profile with D + Q where consistent reductions in immune cell numbers were observed. Animals receiving senolytic therapy demonstrated trends toward decreased total white blood cells ($p=0.097$; Fig. 3a) which resulted from lower numbers across most classes of immune cells after 5 months including circulating neutrophils ($p=0.07$; Fig. 3b) and basophils ($p=0.06$; Fig. 3c), as well as significantly fewer B cells ($p=0.05$, Fig. 3d) and monocytes ($p=0.05$; Fig. 3e) in circulation. CR further reduced circulating neutrophils

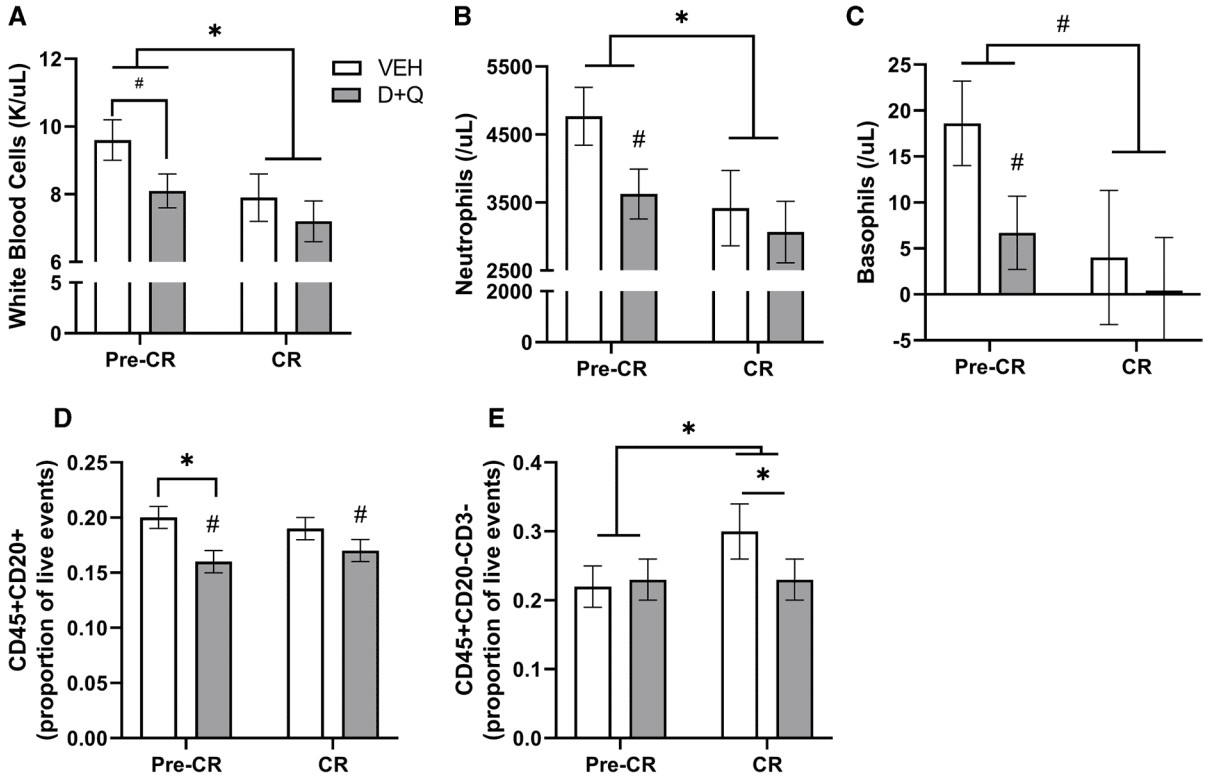

Fig. 3 Senolytic therapy reduces circulating immune cells. After 5 months of intermittent dasatinib (D) and quercetin (Q) administration prior to caloric restriction (Pre-CR), animals receiving senolytic therapy demonstrated trends towards decreases in circulating **A** total white blood cells **B** neutrophils, **C** basophils, and **D** B cells identified as $CD45^{+}CD20^{+}$. However monocytes identified as $CD3^{-}CD20^{-}$ (**E**), showed a significant D + Q × CR interaction whereby D + Q lowered monocytes concurrent with a significant overall effect of CR to increase cell number (* = $p < 0.05$). The effect of CR resulted in general decreases in total white blood cells, neutrophils, and basophilsin both the VEH ($n = 7$) and D + Q ($n = 9$) animals (* = $p < 0.05$; # = $p < 0.1$ vs. Pre-CR). All values presented are adjusted means ± SEM

(CR effect $p = 0.01$), basophils (CR effect $p = 0.07$), and total white blood cells ($p = 0.003$). The combination of intermittent D + Q therapy and CR resulted in maintenance of a healthier immune profile with fewer total circulating monocytes. No shifts in monocyte or macrophage subtypes, or circulating cytokines were seen with D + Q treatment alone (Table 1).

To further understand the observed positive shifts in circulatory immune profiles without changes in circulatory cytokine measures, we evaluated monocyte classes and tissue resident macrophages in adipose. Trends toward increases in non-classical monocytes were observed, leading to an improved ratio of circulating classical to non-classicals in circulation ($p < 0.10$ for all, Supplementary Fig. 5). Overall, CR suppressed intermediate monocytes at month six ($p = 0.01$). Monocytes polarize in a linear fashion and the effect of D + Q can be seen as a shift away from classical toward greater intermediate and non-classical phenotypes (Supplementary Fig. 5). Although no change in total subcutaneous adipose tissue macrophage density was observed (Table 1), D + Q with CR induced a decrease in M2/M1 macrophage ratio ($p = 0.010$; Fig. 4a), indicating a macrophage polarization shift. The difference in M2 macrophage accumulation in the subcutaneous adipose tissue of D + Q and VEH groups can be visually appreciated in Fig. 4c. CR alone resulted in significant decreases in GDF15, also known macrophage inhibitory cytokine-1, in both the VEH and treatment groups ($p = 0.05$; Fig. 4b). As D + Q induces apoptosis and CR incites alterations in adipocytes, we hypothesize that the shift toward M1 polarization coincides with increased clearance of dying adipocytes and released

Table 1 Circulatory cytokine and monocyte profiles, and adipose macrophage measures. Seven vehicle (VEH)-treated control and nine dasatinib (D) and quercetin (Q) intermittently treated middle-aged cynomolgus macaques are reported on at the end of study (−CR) and after 6 additional weeks of caloric restriction (+CR). All values presented are adjusted means ± SEM. * = $p < 0.05$, # = $p < 0.10$

Measurement	VEH -CR	VEH +CR	D + Q -CR	D + Q +CR	D + Q effect *p*-value	CR effect *p*-value	Interaction effect *p*-value
Monocyte chemoattractant protein (MCP)-1 (pg/mL)	109.0 (9.5)	109.9 (12.2)	100.7 (10.1)	86.7 (10.1)	0.23	0.43	0.37
N-terminal-pro hormone BNP (NT-ProBNP) (pg/mL)	298.4 (30.3)	302.5 (35.6)	328.3 (31.3)	295.6 (29.9)	0.67	0.49	0.37
C-reactive protein (CRP) (log ng/mL)	6.4 (0.1)	6.3 (0.1)	6.6 (0.1)	6.4 (0.1)	0.16	0.57	0.41
Circulatory classical monocytes/CD45 + cells	0.12 (0.02)	0.14 (0.02)	0.11 (0.02)	0.09 (0.02)	0.26	0.90	0.29
Circulatory intermediate monocytes/CD45 + cells	0.01 (0.001)	0.02 (0.001)	0.02 (0.001)	0.02 (0.001)	0.65	0.0092	0.042*
Circulatory non-classical monocytes/CD45 + cells	0.06 (0.01)	0.06 (0.01)	0.08 (0.01)	0.08 (0.01)	0.092#	0.74	0.91
SQ adipose cell density (cells/μm^2)	0.0003 (0.0001)	0.0002 (0.0001)	0.0002 (0.00005)	0.0002 (0.0001)	0.35	0.55	0.44
SQ adipose M1 macrophages (%)	1.3 (0.5)	1.1 (0.5)	0.6 (0.4)	1.4 (0.4)	0.32	0.69	0.092
SQ adipose M2 macrophages (%)	50.7 (6.2)	58.4 (6.8)	54.3 (5.5)	43.5 (5.5)	0.67	0.11	0.089#
SQ adipose undefined macrophages (%)	45.7 (6.2)	39.3 (6.7)	43.2 (5.4)	52.5 (5.4)	0.76	0.14	0.15
SQ adipose intermediate macrophages (%)	2.9 (0.8)	1.9 (0.8)	1.5 (0.7)	2.2 (0.7)	0.22	0.73	0.15
SQ adipose macrophage density (cells/μm^2)	0.0000069 (0.000018)	0.0000081 (0.000017)	0.000012 (0.000018)	0.0000090 (0.000018)	0.23	0.94	0.21
SQ adipose adipocyte size (μm^2)	5899.2 (732.4)	7505.2 (910.9)	5511.0 (558.9)	5514.7 (652.0)	0.38	0.11	0.10

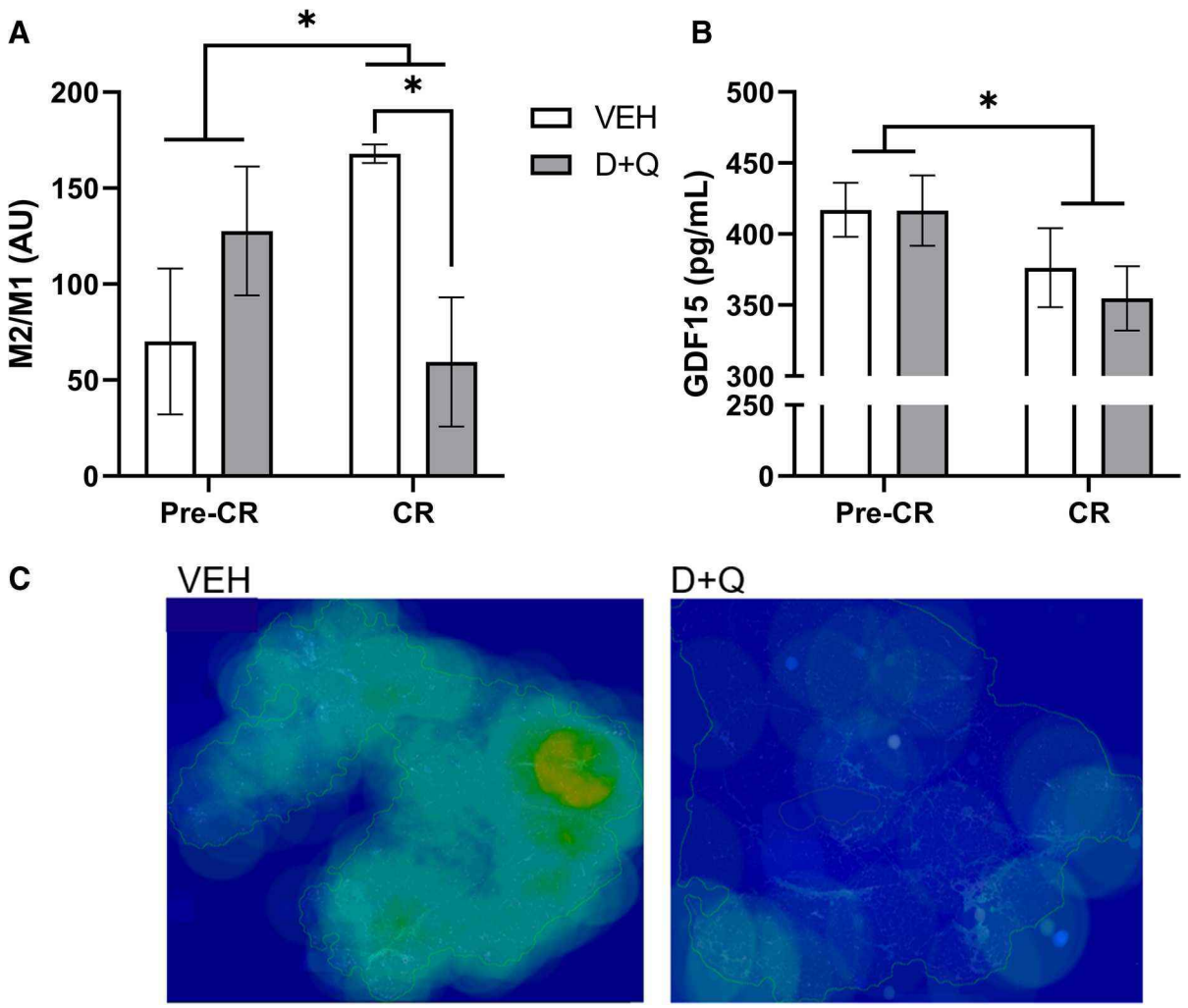

Fig. 4 Senolytic therapy with caloric restriction shifts macrophage polarization. **A** Combined senolytic therapy and caloric restriction resulted in decreased M2/M1 subcutaneous adipose tissue macrophage ratio ($p=0.01$), where M1 macrophage numbers increased and M2 macrophage numbers decreased simultaneously (Table 1). Caloric restriction overall increased M2/M1 ($p=0.05$) driven by VEH animals shifting the macrophage landscape to have fewer M1 and more M2 in their adipose tissue. **B** CR significantly reduced growth differentiation factor (GDF)-15 in both animals receiving VEH ($n=7$) and D + Q ([$n=9$]; $*=p<0.05$). All values presented are adjusted means ± SEM. **C** Representative M2 macrophage AT heat maps, where increasing green to red coloration indicates higher densities of M2 macrophages

free fatty acids to maintain tissue homeostasis. This hypothesis is supported by the large increases in apoptosis-related gene expression observed in D + Q treated animals in month six (Supplementary Fig. 4).

Intestinal barrier and microbiome effects with senolytic therapy and caloric restriction

Loss of intestinal mucosal barrier competency, with translocation of microbial antigens into the portal and systemic circulation, has been a highly conserved and consistent feature of aging [28, 33–35]. Hepatic production of LBP-1 into circulation is a biomarker of this inflammatory process, aiding binding to cell membrane toll-like receptors. D + Q significantly reduced LBP-1 ($p=0.02$, Fig. 5a) which was augmented by the addition of CR. This pattern was replicated in the related biomarkers FABP-1 and IgA (Fig. 5b, c), which substantiate a treatment-related effect on mucosal competency and indicate that CR

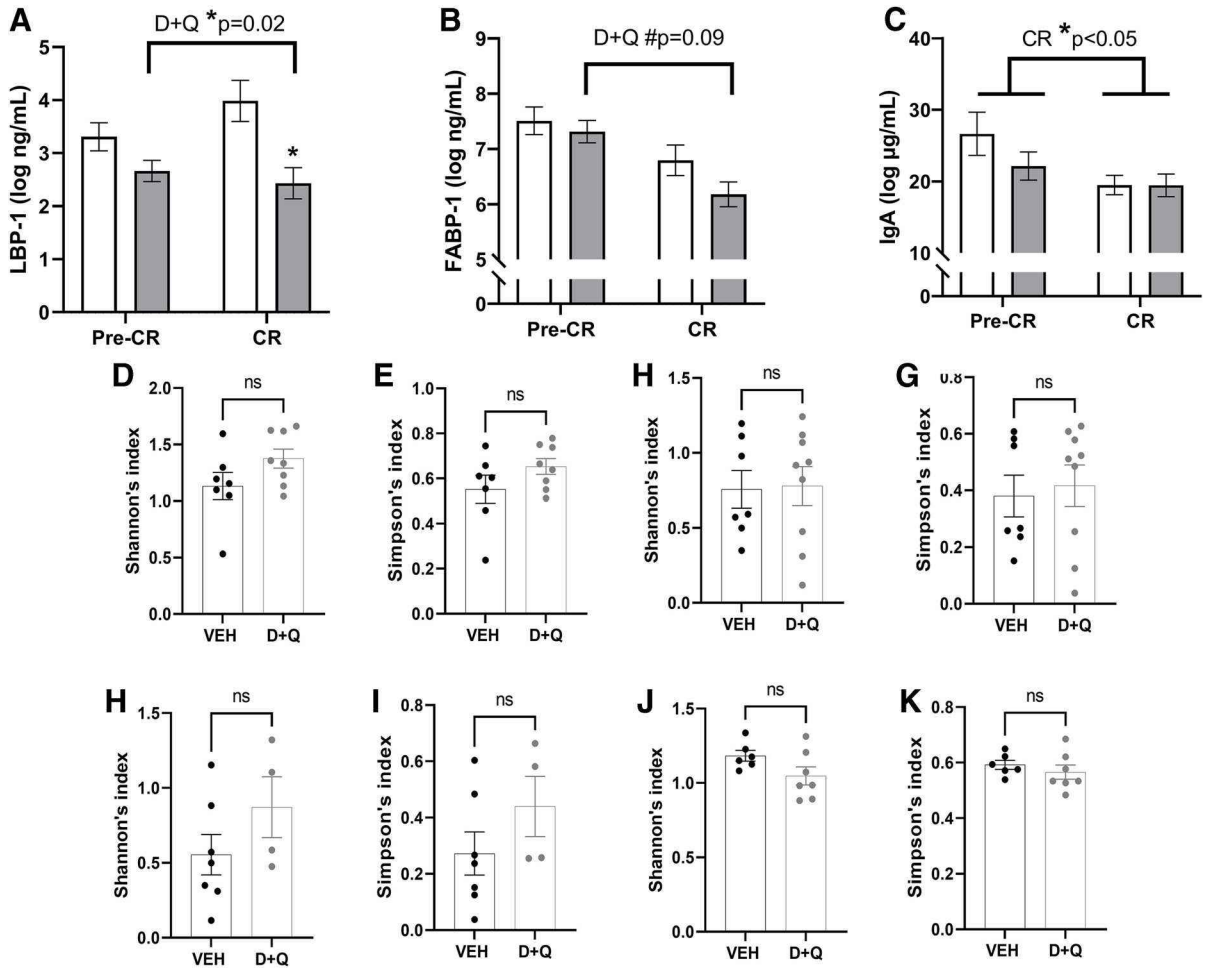

Fig. 5 Senolytic therapy and caloric restriction (CR) improve intestinal barrier biomarkers without changes in the mucosal or fecal microbiomes. **A** Lipopolysaccharide binding protein (LBP)-1 significantly reduced with intermittent dasatinib (D) and quercetin (Q) administration, and an interaction with CR augmented this improvement. **B** Circulatory fatty acid binding protein (FABP)-1 supports intestinal barrier improvements with a trend towards reduced levels across the study. **C**)Immunoglobulin (Ig) A in circulation additionally supports the improvement in intestinal barrier function with D + Q and the positive effect of CR on these endpoints. Colon mucosal microbiome alpha diversity profiles were comparable at baseline (**D**, $p = 0.24$ and **E**, $p = 0.25$) and at study end (6 months; **F**, $p = 0.06$ and **G**, $p = 0.38$) between the vehicle group (VEH) and the dasatinib plus quercetin (D + Q) animals. Similarly, diversity was comparable at study start (**H**, $p = 0.13$ and **I**, $p = 0.19$) and unchanged by treatment (**J**, $p = 0.90$ and *K*, $p = 0.73$) in the fecal microbiome profiles. All values presented are adjusted means ± SEM

provides additional benefit. We also evaluated each individual's microbiome across the study to see if the mucosal barrier was improving with treatment as result of microbial shifts or independently of the microbes colonizing the gut and the colonic mucosal niche. We found no alpha or beta diversity differences in the baseline microbiomes between groups, and no large changes were evident in either niche at study end (Fig. 5D–G, Supplemental Fig. 6). The dominant phyla among all the groups were Firmicutes, Bacteroidetes, Actinobacteria, and Proteobacteria across the time points (Supplemental Fig. 7 and 8). However, none of the taxa showed major differences, but the proportions of each taxon changed with sample type and time point. As for higher taxonomic levels, in feces Firmicutes were higher in the treatment group and Proteobacteria in the control group at baseline and end of study. In mucosa, Bacteroidetes

levels were increased, although non-significantly, in the treatment group at end of study. This suggests that improvements in mucosal barrier function may be related to the tissue epithelial and immune cells, which are key to preventing mucosal-associated microbes from passing to the portal circulation and local intra-abdominal tissues.

Assessments of kidney and liver function with senolytic therapy and caloric restriction

Kidney function often deteriorates with age-related comorbidities related to metabolic syndrome (MetS). Accordingly, we evaluated the impacts of D + Q and CR on measures of kidney function. D + Q alone significantly reduced circulating concentrations of blood urea nitrogen (BUN) after five months ($p = 0.01$; Table 2). Creatinine values remained unchanged throughout the study (Table 2) as did urinary protein:creatinine ratio (data not shown). D + Q alone and with CR did not change liver attenuation values, which are used as a proxy for liver fat accumulation, nor the liver enzymes aspartate aminotransferase (AST) or alkaline phosphatase (ALP) (Table 2). CR significantly increased the liver enzyme alanine aminotransferase (ALT) ($p = 0.0022$), although ALT levels remained in the normal range (Table 2), and we believe this was due to increased sedation events during month six.

Shifts in body composition and metabolic syndrome risk factors with senolytic therapy and caloric restriction

Positive shifts in body composition have been related to improved metabolic health. Here, we determined shifts in body composition and MetS risk factors that were driven by D + Q and/or CR. D + Q alone resulted in a positive trend toward reduced abdominal visceral: subcutaneous adipose ratio ($p = 0.09$) that was driven by an increase in abdominal subcutaneous adipose ($p = 0.10$; Table 3). However, no other body composition changes or alterations to MetS risk factors were the result of D + Q alone.

In line with what has been previously reported, CR significantly decreased bodyweight ($p = 0.0001$), waist circumference ($p = 0.0001$), percentage of total fat mass ($p = 0.02$), and abdominal fat mass ($p = 0.005$), and increased percentage of lean mass ($p = 0.005$; Table 3). Additionally, CR significantly decreased circulating triglycerides ($p = 0.003$), and fasting blood glucose ($p = 0.03$), and demonstrated a trend toward decreasing A1c ($p = 0.07$; Table 3). In sum, these robust CR effects on obesity and related MetS outcomes seen with just 5% of weight loss validate our NHP model as being a good translational model, as these effects mirror what is seen in people. The interaction between D + Q and CR resulted in a significant

Table 2 Renal and hepatic measures. Seven vehicle (VEH)-treated control and nine dasatinib (D) and quercetin (Q) intermittently treated middle-aged cynomolgus macaques are reported on at the end of study (−CR) and after 6 additional weeks of caloric restriction (+CR). A robust improvement in renal blood urea nitrogen (BUN) levels is seen in the treated group. All values presented are adjusted means ± SEM. * = $p < 0.05$, # = $p < 0.10$

Measurement	VEH −CR	VEH +CR	D + Q −CR	D + Q +CR	D + Q effect *p*-value	CR effect *p*-value	Interaction effect *p*-value
Blood urea nitrogen (BUN; mg/dL)	17.3 (0.7)	17.0 (0.8)	14.7 (0.6)	16.1 (0.7)	0.01*	0.25	0.09#
Creatinine (mg/dL)	0.64 (0.03)	0.62 (0.03)	0.65 (0.03)	0.66 (0.03)	0.56	0.69	0.49
BUN:creatinine	27.7 (1.9)	27.9 (2.2)	23.0 (1.7)	25.7 (1.9)	0.14	0.25	0.31
Alanine transaminase (ALT) (U/L)	44.6 (7.1)	60.7 (8.6)	53.7 (6.6)	72.1 (7.6)	0.31	0.0021	0.82
Aspartate aminotransferase (AST) (U/L)	35.8 (2.5)	29.0 (3.3)	32.5 (2.3)	26.6 (2.9)	0.35	0.0097	0.85
Alkaline phosphatase (ALP) (U/L)	90.8 (6.7)	85.5 (7.7)	91.7 (6.2)	81.7 (6.8)	0.95	0.059	0.55
Total protein (g/dL)	6.9 (0.1)	6.9 (0.1)	6.8 (0.1)	7.0 (0.1)	0.53	0.52	0.31
Liver attenuation (HU)	58.7 (2.1)	60.2 (2.3)	62.6 (1.8)	58.6 (1.8)	0.64	0.47	0.13

Table 3 Metabolic syndrome and body composition measures. Seven vehicle (VEH)-treated control and nine dasatinib (D) and quercetin (Q) intermittently treated middle-aged cynomolgus macaques are reported on at the end of study (−CR) and after 6 additional weeks of caloric restriction (+CR). Robust improvement in metabolic syndrome and adiposity measures are seen with CR and 5% mean weight loss (Supplementary Fig. 1). An interaction between D + Q and CR was observed in glycemic control, leading to 0.5% reductions in A1c values in just 6 weeks. All values presented are adjusted means ± SEM. * = $p < 0.05$, # = $p < 0.10$

Measurement	VEH −CR	VEH +CR	D + Q −CR	D + Q +CR	D + Q effect *p*-value	CR effect *p*-value	Interaction effect *p*-value
Body weight (kg)	8.0 (0.1)	7.8 (0.1)	8.1 (0.1)	7.7 (0.1)	0.80	0.0001*	0.14
Waist circumference (cm)	46.7 (1.0)	44.8 (1.0)	47.5 (0.9)	44.4 (0.9)	0.87	0.0001*	0.23
Fasting blood glucose (mg/dL)	146.5 (15.0)	127.0 (18.4)	146.2 (13.2)	115.4 (15.3)	0.83	0.026*	0.60
Glycosylated hemoglobin A1c (%)	5.8 (0.2)	5.9 (0.3)	5.8 (0.2)	5.3 (0.2)	0.48	0.070#	0.03*
Systolic blood pressure (mmHg)	125.6 (7.0)	126.4 (8.3)	127.0 (6.2)	130.6 (6.9)	0.81	0.62	0.75
Diastolic blood pressure (mmHg)	68.6 (4.2)	80.6 (5.5)	73.2 (3.7)	79.2 (4.5)	0.65	0.020*	0.41
Triglycerides (log mg/dL)	5.3 (0.2)	5.1 (0.2)	5.4 (0.2)	4.9 (0.2)	0.94	0.0026*	0.13
High-density lipoprotein cholesterol (mg/dL)	44.2 (2.5)	45.4 (2.6)	47.9 (2.2)	49.3 (2.2)	0.22	0.43	0.96
Fat mass % body weight	32.5 (1.2)	31.5 (1.3)	32.4 (1.1)	30.3 (1.1)	0.70	0.022*	0.32
Lean mass % body weight	46.0 (1.1)	47.3 (1.1)	47.6 (1.0)	49.8 (1.0)	0.20	0.0052*	0.43
Abdominal fat mass (kg)	1.1 (0.1)	1.0 (0.1)	1.1 (0.1)	1.1 (0.1)	0.79	0.0046*	0.41
Psoas area (cm^2)	1.4 (0.1)	1.5 (0.1)	1.2 (0.1)	1.3 (0.1)	0.16	0.095#	0.92
Abdominal visceral: subcutaneous adipose (cm^3)	1.5 (0.1)	1.5 (0.1)	1.2 (0.1)	1.3 (0.1)	0.08	0.15	0.09
Abdominal subcutaneous adipose volume (cm^3)	0.51 (0.05)	0.48 (0.05)	0.54 (0.04)	0.49 (0.04)	0.75	0.0001*	0.10#
Abdominal visceral adipose volume (cm^3)	0.59 (0.05)	0.56 (0.05)	0.59 (0.04)	0.56 (0.04)	0.99	0.12	0.75

decrease in glycosylated hemoglobin A1c ($p = 0.03$; Table 3). No other changes in either body composition or MetS were impacted by the interaction between D + Q and CR.

Shifts in Alzheimer's disease biomarkers with senolytic therapy and caloric restriction

The ratio of $A\beta_{42}$/ $A\beta_{40}$ remained unchanged throughout the study, suggesting that senolytic D + Q treatment had neutral effects in this middle-aged NHP cohort (Supplementary Table 6). We did observe reductions in CSF $A\beta_{40}$ levels with D + Q treatment ($p = 0.02$) and reductions in CSF $A\beta_{42}$ levels as an effect of CR ($p = 0.03$).

Discussion

There is an unmet need in the geroscience community for safe and effective interventions that target multiple pathways known to drive age-related tissue dysfunction [2]. There is also a related gap in the timely translation of target compound outcomes from in silica and preclinical models to human and nonhuman primate studies [36]. Herein, we attempt to provide outcomes and broad multi-systemic assessments regarding the most commonly assessed senolytic combination investigated to date. This study is the first to compare the effects of senolytic therapy on metabolic health outcomes to a proven method of ameliorating metabolic dysfunction, caloric restriction [37]. This study also represents a first long-term

exposure to D + Q with reporting of any pharmacokinetic and pharmacodynamic outcomes where we find that the currently preferred dose of dasatinib resulted in circulatory concentrations less than a third of those used in vitro and we confirm the low bioavailability of quercetin. However, we do confirm that D + Q effect reductions in senescence-associated gene expressions in adipose tissue.

Herein, biosystems that are thought to contribute to age- and metabolic-related physiological dysfunction are surveyed; namely shifts in MetS risk criteria, intestinal leakiness and barrier function, immune cells and selected circulating cytokines, Alzheimer's disease biomarkers, adipose tissue macrophages and tissue insulin signaling driven by D + Q, caloric restriction, and the interaction between the two interventions thought to improve health and lifespan. The 6-month duration of this preclinical trial is relevant to human clinical trials, and these data provide preliminary evidence of safety, effect sizes, and how to direct the enrollment in future clinical trial designs. For this work, we used a translationally relevant NHP model that demonstrates spontaneous obesity and type II diabetes [36, 38]. Our middle-aged NHP cohort included both obese and metabolically unhealthy animals, and, as an animal model able to respond effectively to calorie restriction and, in line with previous reporting [39], did so here.

We determined that the effects of the chosen D + Q dose are primarily seen with intestinal leakiness, kidney parameters and immune cell shifts. Overall, outcomes including liver enzyme evaluations verify that intermittent D + Q administration is safe in NHPs although transient post-dose nausea was observed as has been reported clinically [10]. D + Q alone successfully reduced the gene expressions of cell cycle inhibitor proteins p16 and p21 in subcutaneous adipose tissue at months one and three. Our previous work indicated that whole tissue explant SA-βgal staining may not be sensitive enough to determine differences between groups [22]. While tissue-limited in this study, future work will include SA-βgal staining of the stromal vascular fraction of adipose tissue, as adipose tissue macrophages, endothelial cells, and preadipocytes have been identified as being senescent [40].

A key takeaway from our study is that antigenic stimuli and circulatory leukocyte profiles suggest an anti-inflammatory effect of D + Q that is potentiated in the context of mild and, importantly, clinically achievable levels of CR. Improved intestinal barrier function has been seen in animal models with quercetin and D + Q, [7, 41] and with CR [42] and our data confirms that these effects on microbial translocation biomarkers exist independently of shifts in the microbiome. Stable microbiomes are expected based on studies of people when diet and environments are consistent [43]. Limitations to our microbiome assessments include only two sample types (mucosal tissue and fecal) in the lower intestine; however, this is the most microbe-rich region of the body and these sites are known to have distinct microbial profiles [44], which shift in aged NHPs and people, and drive metabolic disease [28, 43].

Five months of D + Q treatment successfully improved kidney parameters and demonstrated trends toward improving abdominal adipose tissue distribution, which was observed previously [5, 11, 13, 45], indicating that these agents may be prioritized for treatment of diabetes and diabetic kidney disease. D + Q treatment alone reduced total circulatory white cell counts and proportions of activated monocytes and demonstrated trends toward reducing circulating neutrophils and basophils. It is possible that D + Q treatment dampens aberrant bone marrow activation, which properly resets leukocyte populations, as bone marrow activation has been shown to be highly associated with MetS components and atherosclerosis development [46, 47]. Dasatinib is known to induce myelosuppresion in chemotherapeutic dose regimens; however, the changes observed with intermittent exposure were small reductions and values remained within reference normal ranges for this species. D + Q alone did not result in changes in either circulating cytokines or density of adipose tissue macrophages. However, the concentration of D applied ex vivo directly to adipose tissue explants that resulted in decreased cytokine expression was 1uM — roughly 80% higher than *our* in vivo *circulatory concentration measures, indicating that our* in vivo tissue concentrations may have been too low to incite systemic cytokine shifts [12]. As there was variability in the concentrations of D and its metabolites measured, it is also possible that differences in bioavailability may result in response heterogeneity. We collected adipose biopsies roughly 28–30 days post-D + Q administration and shifts in macrophage density or subtype may have been missed or require more frequent D + Q

administrations than monthly exposure, as Hickson et al. demonstrated decreases in adipose tissue macrophages 11 days after D + Q dosing [11].

White adipose tissue acts an endocrine organ, where adipocytes detect, process, and propagate signals to maintain energy equilibrium and, along with immune cells, secrete bioactive hormones, cytokines and signaling proteins that regulate metabolism [48]. In healthy states, white adipose demonstrates a balanced profile of total adipose tissue macrophages across the inflammatory spectrum, from pro-inflammatory M1 to anti-inflammatory M2 macrophages, to maintain metabolic homeostasis [49]. Immune cells, preadipocytes, and endothelial cells become senescent in white adipose, and drive insulin resistance in obese states [40]. Both D + Q and CR cause adipocyte turnover. Our data suggests the combination of D + Q and CR resulted in increased adipocyte necrosis and death, which caused an increase in p21 expression in surrounding cells and a corresponding shift in macrophage polarization from M2 to M1. Adipocyte death has been shown to result in pro-inflammatory metabolic activation of macrophages that is accompanied by increased expression of genes associated with M1-polarization [50]. This macrophage flexibility may be part of a coordinated response to maintain adipose health and function [50, 51]. Similarly, p21 expression acts as a mechanism of immunosurveillance and results in polarization of M1 macrophages, which recruit cytotoxic T cells that facilitate targeted cell removal to maintain tissue homeostasis [52]. Therefore, we hypothesize, given the positive decreases in MetS risk factors and circulating immune cells observed with D + Q combined with CR and our apoptosis-related gene expression data that the increase in p21 and the corresponding macrophage polarization shift positively contributed to tissue homeostasis maintenance and healthy adipocyte turnover.

The changes in adipose features seen with D + Q + CR were seen concomitant with large reductions in A1c, and although D alone is able to reduce blood glucose [53], benefits were only observed with concurrent CR and shifts in adipose senescence and immune cell markers. The interaction between CR and D + Q therapy also resulted in reductions in circulating monocytes, in particular significant decreases in intermediate and non-significant decreases in classical monocytes, as well as unexpected shifts in senescence markers and adipose tissue macrophages. The decrease in total monocytes supports previous senolytic-related work [13], although this study is the first to delineate which specific monocyte subtypes were altered.

Future directions for this work include broadening our cell-specific investigations and the duration of the caloric restriction component of the study. It is well-documented that not all cells that are p16-, p21-, and SA-βgal-positive are senescent [54–57] and recently, p19 has been shown to be a preferred marker for brain senescence [57]. The reduction in Alzheimer's biomarker $A\beta_{42}$ in CSF following CR invite investigation into this intervention's effects on production, aggregation and clearance of $A\beta_{42}$, as reductions in $A\beta_{42}$ in CSF following diet change have also been observed in middle-aged people [58]. The neutral effect of D + Q on the preferred CSF biomarker, $A\beta_{42/40}$, warrants future investigations into CSF biomarkers relating to tau [57].

This study incorporated a six-week caloric restriction in both groups (VEH and D + Q). We recognize that we were not able to include an ad-libitum fed only group due to limited animal availability and that the gold standard for caloric restriction duration in human clinical trials is 24 weeks. In a longer trial with a 24-week caloric restriction combined with intermittent D + Q therapy and a caloric restriction-only group, we believe that we may see additional differences, including re-establishment of preferred adipose tissue markers [27]. In a larger trial, sex differences could also be evaluated, as the group sizes in this work did not permit this analysis. Given the outcomes of this study, we believe that these data provide preliminary evidence to support safe implementation of a human clinical trial, perhaps focused on diabetic kidney disease in mid-to-late-age adults. We believe that intermittent D + Q combined with low-percentage caloric restriction would significantly and safely ameliorate inflammation, glycemia and renal outcomes associated with metabolic dysfunction related to aging.

Acknowledgements The authors would like to recognize the technicians involved in the care of the study animals, and the animals that made this study possible. Special acknowledgement for Dr. Miranda Orr for her assistance in the review and interpretation of data.

Author contribution Authors involved in data generation and data analysis: ADR, AW, DD, HC, SM, SD, JJ, KK. Authors involved in sample collection and trial conductance: ADR, MB, RV, KK, AW. Authors involved in manuscript writing and editing: ADR, KK, SM.

Funding The authors received funding from R01HL142930, P40OD010965, ULTR001420, T32AI007401, and T35OD010946.

Data Availability All data will be made available upon request.

Declarations

Conflict of interest The authors declare no conflicts of interest.

References

1. Kennedy BK, Berger SL, Brunet A, Campisi J, Cuervo AM, Epel ES, Franceschi C, Lithgow GJ, Morimoto RI, Pessin JE. Aging: a common driver of chronic diseases and a target for novel interventions. Cell. 2014;159(4):709.
2. López-Otín C, Blasco MA, Partridge L, Serrano M, Kroemer G. The hallmarks of aging. Cell. 2013;153(6):1194–217.
3. Prata LGL, Ovsyannikova IG, Tchkonia T, Kirkland JL, editors. Senescent cell clearance by the immune system: emerging therapeutic opportunities. Seminars in immunology; 2018: Elsevier.
4. Zhu Y, Tchkonia T, Pirtskhalava T, Gower AC, Ding H, Giorgadze N, Palmer AK, Ikeno Y, Hubbard GB, Lenburg M. The Achilles' heel of senescent cells: from transcriptome to senolytic drugs. Aging Cell. 2015;14(4):644–58.
5. Xu J, Zhou L, Liu Y. Cellular senescence in kidney fibrosis: pathologic significance and therapeutic strategies. Front Pharmacol. 2020;11:1898.
6. Baker DJ, Wijshake T, Tchkonia T, LeBrasseur NK, Childs BG, Van De Sluis B, Kirkland JL, Van Deursen JM. Clearance of p16Ink4a-positive senescent cells delays ageing-associated disorders. Nature. 2011;479(7372):232–6.
7. Saccon TD, Nagpal R, Yadav H, Cavalcante MB, Nunes ADC, Schneider A, Gesing A, Hughes B, Yousefzadeh M, Tchkonia T, Kirkland JL, Niedernhofer LJ, Robbins PD, Masternak MM. Senolytic combination of dasatinib and quercetin alleviates intestinal senescence and inflammation and modulates the gut microbiome in aged mice. J Gerontol A Biol Sci Med Sci. 2021;76(11):1895–905. https://doi.org/10.1093/gerona/glab002.
8. Ota H, Kodama A. Dasatinib plus quercetin attenuates some frailty characteristics in SAMP10 mice. Sci Rep. 2022;12(1):2425. https://doi.org/10.1038/s41598-022-06448-5.
9. Dungan CM, Figueiredo VC, Wen Y, VonLehmden GL, Zdunek CJ, Thomas NT, Mobley CB, Murach KA, Brightwell CR, Long DE, Fry CS, Kern PA, McCarthy JJ, Peterson CA. Senolytic treatment rescues blunted muscle hypertrophy in old mice. Geroscience. 2022;44(4):1925–40. https://doi.org/10.1007/s11357-022-00542-2.
10. Justice JN, Nambiar AM, Tchkonia T, LeBrasseur NK, Pascual R, Hashmi SK, Prata L, Masternak MM, Kritchevsky SB, Musi N, Kirkland JL. Senolytics in idiopathic pulmonary fibrosis: results from a first-in-human, open-label, pilot study. EBioMedicine. 2019;40:554–63. https://doi.org/10.1016/j.ebiom.2018.12.052.
11. Hickson LJ, Prata LGL, Bobart SA, Evans TK, Giorgadze N, Hashmi SK, Herrmann SM, Jensen MD, Jia Q, Jordan KL. Senolytics decrease senescent cells in humans: preliminary report from a clinical trial of dasatinib plus quercetin in individuals with diabetic kidney disease. EBioMedicine. 2019;47:446–56.
12. Xu M, Pirtskhalava T, Farr JN, Weigand BM, Palmer AK, Weivoda MM, Inman CL, Ogrodnik MB, Hachfeld CM, Fraser DG. Senolytics improve physical function and increase lifespan in old age. Nat Med. 2018;24(8):1246–56.
13. Palmer AK, Xu M, Zhu Y, Pirtskhalava T, Weivoda MM, Hachfeld CM, Prata LG, van Dijk TH, Verkade E, Casaclang-Verzosa G. Targeting senescent cells alleviates obesity-induced metabolic dysfunction. Aging Cell. 2019;18(3):e12950.
14. Branch-Mays GL, Dawson DR, Gunsolley JC, Reynolds MA, Ebersole JL, Novak KF, Mattison JA, Ingram DK, Novak MJ. The effects of a calorie-reduced diet on periodontal inflammation and disease in a non-human primate model. J Periodontol. 2008;79(7):1184–91.
15. Messaoudi I, Warner J, Fischer M, Park B, Hill B, Mattison J, Lane MA, Roth GS, Ingram DK, Picker LJ. Delay of T cell senescence by caloric restriction in aged long-lived nonhuman primates. Proc Natl Acad Sci. 2006;103(51):19448–53.
16. Kastman EK, Willette AA, Coe CL, Bendlin BB, Kosmatka KJ, McLaren DG, Xu G, Canu E, Field AS, Alexander AL. A calorie-restricted diet decreases brain iron accumulation and preserves motor performance in old rhesus monkeys. J Neurosci. 2010;30(23):7940–7.
17. Civitarese AE, Carling S, Heilbronn LK, Hulver MH, Ukropcova B, Deutsch WA, Smith SR, Ravussin E. Calorie restriction increases muscle mitochondrial biogenesis in healthy humans. PLoS Med. 2007;4(3):e76.
18. Colman RJ, Beasley TM, Allison DB, Weindruch R. Attenuation of sarcopenia by dietary restriction in rhesus monkeys. J Gerontol A Biol Sci Med Sci. 2008;63(6):556–9.
19. Most J, Tosti V, Redman LM, Fontana L. Calorie restriction in humans: an update. Ageing Res Rev. 2017;39:36–45.
20. Krishnamurthy J, Torrice C, Ramsey MR, Kovalev GI, Al-Regaiey K, Su L, Sharpless NE. Ink4a/Arf expression is a biomarker of aging. J Clin Investig. 2004;114(9):1299–307.
21. Bacarella N, Ruggiero A, Davis AT, Uberseder B, Davis MA, Bracy DP, Wasserman DH, Cline JM, Sherrill C, Kavanagh K. Whole body irradiation induces diabetes and adipose insulin resistance in nonhuman primates. Int J Radiat Oncol Biol Phys. 2020;106(4):878–86.

22. Kavanagh K, Sherrill C, Ruggiero A, Block M, Vemuri R, Davis M, Olivier A. Biomarkers of senescence in non-human primate adipose depots relate to aging. GeroScience. 2021;43(1):343–52.
23. Ruggiero AD, Davis A, Sherrill C, Westwood B, Hawkins GA, Palmer ND, Chou JW, Reeves T, Cox LA, Kavanagh K. Skeletal muscle extracellular matrix remodeling with worsening glycemic control in nonhuman primates. Am J Physiol-Regul Integr Comp Physiol. 2021;320(3):R226–35.
24. Kavanagh K, Dendinger MD, Davis AT, Register TC, DeBo R, Dugan G, Cline JM. Type 2 diabetes is a delayed late effect of whole-body irradiation in nonhuman primates. Radiat Res. 2015;183(4):398–406.
25. Kavanagh K, Davis AT, Peters DE, LeGrand AC, Bharadwaj MS, Molina AJ. Regulators of mitochondrial quality control differ in subcutaneous fat of metabolically healthy and unhealthy obese monkeys. Obesity. 2017;25(4):689–96.
26. Vemuri R, Ruggiero A, Whitfield JM, Dugan GO, Cline JM, Block MR, Guo H, Kavanagh K. Hypertension promotes microbial translocation and dysbiotic shifts in the fecal microbiome of nonhuman primates. Am J Physiol-Heart Circ Physiol. 2022;322(3):H474–85.
27. Ruggiero AD, Vemuri R, Block M, DeStephanis D, Davis M, Chou J, Williams A, Brock A, Das SK, Kavanagh K. Macrophage phenotypes and gene expression patterns are unique in naturally occurring metabolically healthy obesity. Int J Mol Sci. 2022;23(20). https://doi.org/10.3390/ijms232012680.
28. Vemuri R, Sherrill C, Davis MA, Kavanagh K. Age-related colonic mucosal microbiome community shifts in monkeys. J Gerontol A Biol Sci Med Sci. 2021;76(11):1906–14. https://doi.org/10.1093/gerona/glaa256.
29. Kavanagh K, Day SM, Pait MC, Mortiz WR, Newgard CB, Ilkayeva O, Mcclain DA, Macauley SL. Type-2-diabetes alters CSF but not plasma metabolomic and AD risk profiles in vervet monkeys. Front Neurosci. 2019;13:89.
30. Bero AW, Yan P, Roh JH, Cirrito JR, Stewart FR, Raichle ME, Lee J-M, Holtzman DM. Neuronal activity regulates the regional vulnerability to amyloid-β deposition. Nat Neurosci. 2011;14(6):750–6.
31. Roh JH, Huang Y, Bero AW, Kasten T, Stewart FR, Bateman RJ, Holtzman DM. Disruption of the sleep-wake cycle and diurnal fluctuation of β-amyloid in mice with Alzheimer's disease pathology. Sci Transl Med. 2012;4(150):150ra22-ra22.
32. Kavanagh K, Sherrill C, Ruggiero A, Block M, Vemuri R, Davis M, Olivier A. Biomarkers of senescence in non-human primate adipose depots relate to aging. Geroscience. 2021;43(1):343–52. https://doi.org/10.1007/s11357-020-00230-z.
33. Kavanagh K, Brown RN, Davis AT, Uberseder B, Floyd E, Pfisterer B, Shively CA. Microbial translocation and skeletal muscle in young and old vervet monkeys. Age (Dordr). 2016;38(3):58. https://doi.org/10.1007/s11357-016-9924-z.
34. Kavanagh K, Hsu F-C, Davis AT, Kritchevsky SB, Rejeski WJ, Kim S. Biomarkers of leaky gut are related to inflammation and reduced physical function in older adults with cardiometabolic disease and mobility limitations. GeroSci. 2019;Online first. https://doi.org/10.1007/s11357-019-00112-z.
35. Man AL, Gicheva N, Nicoletti C. The impact of ageing on the intestinal epithelial barrier and immune system. Cell Immunol. 2014;289(1–2):112–8. https://doi.org/10.1016/j.cellimm.2014.04.001.
36. Kirkland JL, Tchkonia T. Clinical strategies and animal models for developing senolytic agents. Exp Gerontol. 2015;68:19–25. https://doi.org/10.1016/j.exger.2014.10.012.
37. Wycherley T, Brinkworth GD, Noakes M, Buckley JD, Clifton PM. Effect of caloric restriction with and without exercise training on oxidative stress and endothelial function in obese subjects with type 2 diabetes. Diabetes Obes Metab. 2008;10(11):1062–73.
38. Wagner JD, Kavanagh K, Ward GM, Auerbach BJ, Harwood HJ Jr, Kaplan JR. Old world nonhuman primate models of type 2 diabetes mellitus. ILAR J. 2006;47(3):259–71.
39. Cefalu WT, Wagner JD, Wang ZQ, Bell-Farrow AD, Collins J, Haskell D, Bechtold R, Morgan T. A study of caloric restriction and cardiovascular aging in cynomolgus monkeys (*Macaca fascicularis*): A Potential Model for Aging Research. J Gerontol A Biol Sci Med Sci. 1997;52(1):B10–9.
40. Wang L, Wang B, Gasek NS, Zhou Y, Cohn RL, Martin DE, Zuo W, Flynn WF, Guo C, Jellison ER. Targeting p21Cip1 highly expressing cells in adipose tissue alleviates insulin resistance in obesity. Cell Metab. 2022;34(1):75-89.e8.
41. Sun L, Guo L, Xu G, Li Z, Appiah MO, Yang L, Lu W. Quercetin reduces inflammation and protects gut microbiota in broilers. Molecules. 2022;27(10). https://doi.org/10.3390/molecules27103269.
42. Ma TY, Hollander D, Dadufalza V, Krugliak P. Effect of aging and caloric restriction on intestinal permeability. Exp Gerontol. 1992;27(3):321–33.
43. Claesson MJ, Cusack S, O'Sullivan O, Greene-Diniz R, de Weerd H, Flannery E, Marchesi JR, Falush D, Dinan T, Fitzgerald G, Stanton C, van Sinderen D, O'Connor M, Harnedy N, O'Connor K, Henry C, O'Mahony D, Fitzgerald AP, Shanahan F, Twomey C, Hill C, Ross RP, O'Toole PW. Composition, variability, and temporal stability of the intestinal microbiota of the elderly. Proc Natl Acad Sci U S A. 2011;108(Suppl 1):4586–91. https://doi.org/10.1073/pnas.1000097107.
44. Lyra A, Forssten S, Rolny P, Wettergren Y, Lahtinen SJ, Salli K, Cedgard L, Odin E, Gustavsson B, Ouwehand AC. Comparison of bacterial quantities in left and right colon biopsies and faeces. World J Gastroenterol. 2012;18(32):4404–11. https://doi.org/10.3748/wjg.v18.i32.4404.
45. Huang W, Hickson LJ, Eirin A, Kirkland JL, Lerman LO. Cellular senescence: the good, the bad and the unknown. Nat Rev Nephrol. 2022;18(10):611–27. https://doi.org/10.1038/s41581-022-00601-z.
46. Devesa A, Lobo-González M, Martínez-Milla J, Oliva B, García-Lunar I, Mastrangelo A, España S, Sanz J, Mendiguren JM, Bueno H. Bone marrow activation in

response to metabolic syndrome and early atherosclerosis. Eur Heart J. 2022;43(19):1809–28.
47. Santopaolo M, Sullivan N, Thomas AC, Alvino VV, Nicholson LB, Gu Y, Spinetti G, Kallikourdis M, Blom A, Madeddu P. Activation of bone marrow adaptive immunity in type 2 diabetes: Rescue by co-stimulation modulator Abatacept. Front Immunol. 2021;12:353.
48. Trzeciak-Ryczek A, Tokarz-Deptuła B, Niedźwiedzka-Rystwej P, Deptuła W. Review paper Adipose tissue–component of the immune system. Cent Eur J Immunol. 2011;36(2):95–9.
49. Wculek SK, Dunphy G, Heras-Murillo I, Mastrangelo A, Sancho D. Metabolism of tissue macrophages in homeostasis and pathology. Cell Mol Immunol. 2022;19(3):384–408.
50. Lindhorst A, Raulien N, Wieghofer P, Eilers J, Rossi F, Bechmann I, Gericke M. Adipocyte death triggers a pro-inflammatory response and induces metabolic activation of resident macrophages. Cell Death Dis. 2021;12(6):1–15.
51. Wernstedt Asterholm I, Tao C, Morley TS, Wang QA, Delgado-Lopez F, Wang ZV, Scherer PE. Adipocyte inflammation is essential for healthy adipose tissue expansion and remodeling. Cell Metab. 2014;20(1):103–18. https://doi.org/10.1016/j.cmet.2014.05.005.
52. Sturmlechner I, Zhang C, Sine CC, van Deursen E-J, Jeganathan KB, Hamada N, Grasic J, Friedman D, Stutchman JT, Can I. p21 produces a bioactive secretome that places stressed cells under immunosurveillance. Science. 2021;374(6567):eabb3420.
53. Agostino NM, Chinchilli VM, Lynch CJ, Koszyk-Szewczyk A, Gingrich R, Sivik J, Drabick JJ. Effect of the tyrosine kinase inhibitors (sunitinib, sorafenib, dasatinib, and imatinib) on blood glucose levels in diabetic and nondiabetic patients in general clinical practice. J Oncol Pharm Pract. 2011;17(3):197–202. https://doi.org/10.1177/1078155210378913.
54. Hall BM, Balan V, Gleiberman AS, Strom E, Krasnov P, Virtuoso LP, Rydkina E, Vujcic S, Balan K, Gitlin II. p16 (Ink4a) and senescence-associated β-galactosidase can be induced in macrophages as part of a reversible response to physiological stimuli. Aging (Albany NY). 2017;9(8):1867.
55. Huang T, Rivera-Pérez JA. Senescence-associated β-galactosidase activity marks the visceral endoderm of mouse embryos but is not indicative of senescence. Genesis. 2014;52(4):300–8.
56. Idda ML, McClusky WG, Lodde V, Munk R, Abdelmohsen K, Rossi M, Gorospe M. Survey of senescent cell markers with age in human tissues. Aging (Albany NY). 2020;12(5):4052.
57. Dehkordi SK, Walker J, Sah E, Bennett E, Atrian F, Frost B, Woost B, Bennett RE, Orr TC, Zhou Y, Andhey PS, Colonna M, Sudmant PH, Xu P, Wang M, Zhang B, Zare H, Orr ME. Profiling senescent cells in human brains reveals neurons with CDKN2D/p19 and tau neuropathology. Nat Aging. 2021;1(12):1107–16. https://doi.org/10.1038/s43587-021-00142-3.
58. Bayer-Carter JL, Green PS, Montine TJ, VanFossen B, Baker LD, Watson GS, Bonner LM, Callaghan M, Leverenz JB, Walter BK. Diet intervention and cerebrospinal fluid biomarkers in amnestic mild cognitive impairment. Arch Neurol. 2011;68(6):743–52.